Local Atomic and Electronic Structure of Boron Chemical Doping in Monolayer Graphene

Supporting Information

Liuyan Zhao[†], Mark P. Levendorf[‡], Scott Goncher[‖], Theanne Schiros[§], Lucia Pálová[‖], Amir Zabet-Khosousi[‖], Kwang Taeg Rim[‖], Christopher Gutiérrez[†], Dennis Nordlund[¥], Cherno Jaye[•], Mark Hybertsen[¶], David Reichman[‖], George W. Flynn[‖], Jiwoong Park[‡], Abhay N. Pasupathy[†].

[†]Department of Physics, Columbia University, New York, New York, 10027, United States
[‡]Chemistry Department, Cornell University, Ithaca, New York, 10065
[‖]Chemistry Department, Columbia University, New York, New York, 10027
[§]Energy Frontier Research Center, Columbia University, New York, New York, 10027, United States
[¥]Stanford Synchrotron Radiation Lightsource, SLAC National Accelerator Laboratory, Menlo Park, California 94025, USA
[•]Materials Measurement Laboratory, National Institute of Standards and Technology, Gaithersburg, Maryland 20899, United States.
[¶]Center for Functional Nanomaterials, Brookhaven National Laboratory, Upton, New York, 11973 United States

Contents:

S1. Line profiles across graphitic B and N dopants without normalization

As shown in Fig. S1, the apparent heights at graphitic B and N dopants are ~1.02Å and ~0.66Å, respectively.

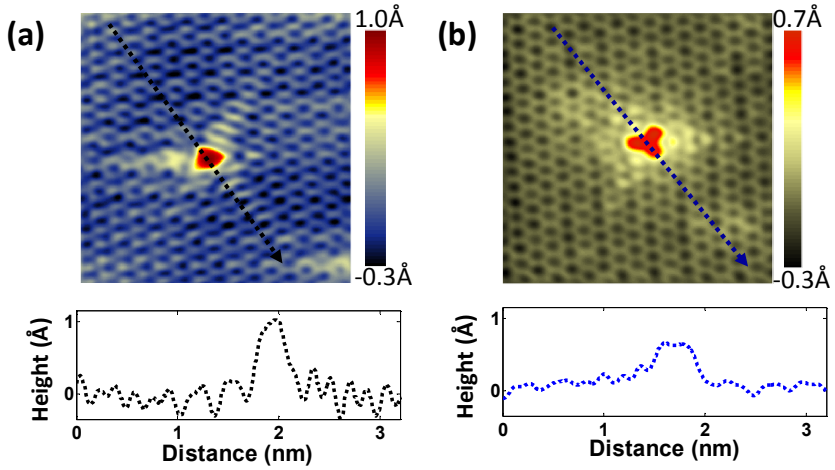

Fig. S1. (a) and (b) Upper panel: STM topographic images taken at single graphitic B and N dopant respectively. Lower panel: Line profile taken across graphitic B and N dopant respectively.

S2. DFT simulations of B/N-doped graphene with and without a Cu(111) substrate

First-principles calculations are performed using density functional theory (DFT) within the local density approximation (LDA) as implemented in the Quantum Espresso (QE) package[1].

For the STM image simulations on a model of free-standing graphene, norm conserving pseudopotentials with Perdew-Zunger (PZ) fit of the Ceperley-Alder electron gas results for exchange and correlation provided with the package (Von Barth-Car direct-fit) are used for the STM image simulations with 3 valence electrons for boron and 4 valence electrons for carbon and with the energy cutoff for the plane-wave basis set to 95 Ry. The STM image simulations were carried out using the Tersoff-Hamann approach[2]. We apply a bias voltage of +0.5 eV; hence we probe the B-doped graphene empty states. The STM image simulation in Fig. 1b was calculated on an 8x8 B doped graphene supercell with 128 atoms.

We calculate the hole concentration shown in Fig. 3d using the formula and parameters described in the text. Following the experimental protocol, the value of the Dirac point has been evaluated from the minimum in the total density of states. We use 7x7 (98 atoms), 11x11 (242 atoms) supercells with 1 B atom and 12x12 supercell (288 atoms) with 1, 2 and 5 B atoms evenly distributed (equivalent to a 12x12, 6x6 and ~3.8x3.8 supercell with 1B atom, respectively) in order to arrive at a varying B concentration. We find that the free carrier concentration varies between 3.7 (for the 12x12 cell with 5B dopants) to 0.9 x 10^{13} cm^{-2} (for the 12x12 cell with 1B dopant). We estimate the average ratio of the deduced free hole concentration to the B concentration to be 57%. For these calculations, we use Vanderbilt ultrasoft pseudopotentials[3] with PBE exchange-correlation functional as provided and implemented in the QE package. We use an energy cutoff of 30 Ry, and a uniform 6x6 Monkhorst-type k-point grids with zero offsets.

To probe interactions with the Cu substrate, we model an underlying Cu(111) substrate using four Cu layers. We utilize ultrasoft pseudopotentials (A. Dal Corso) with PZ exchange-correlation functional as implemented in the QE package with 11, 5, 4 and 3 valence electrons for Cu, N, C and B, respectively. The energy cutoff is 25 Ry. A uniform (3x3x1) Monkhorst-Pack k-point grid with zero offset is used. We strain the Cu substrate to the lattice constant 2.44 Å of pristine graphene. This way, we focus our attention to the impact of the Cu states on the electronic properties of unstrained graphene. We introduce substitutional N or B into the graphene lattice and we perform structural relaxation until the forces are less than 10^{-3} Ry/a.u. We use 4x4 interface supercells. We observe that N remains coplanar with the surrounding graphene, with the N-C nearest neighbor distance 1.40 Å, whereas B comes closer to the Cu substrate due to a stronger B-Cu interaction. The relaxed C-Cu distance in pristine graphene is 3.32 Å. This distance is about the same in N doped graphene, d(N-Cu)=3.35 Å, but considerably smaller in B doped graphene, d(B-Cu)=2.39 Å compared to d(C_nn-Cu)=2.78Å for the nearest neighbor C atom. We obtain charge density differences (CDD) and projected density of states (pDOS) near the Fermi energy as shown in Figs. S2 and S3. We visualize the loss (blue) or gain (red) of the charge by comparing the B/N doped electronic charge density to a pristine graphene reference (we substitute N/B atoms by C atoms without relaxing the atomic positions). Thus, the resulting CDDs are calculated according to: $\rho_{diff} = \rho_{doped} - \rho_{pristine}$.

We investigate the importance of the location of the N/B atom relative to the Cu(111) surface lattice by studying three different types of registry for the N and B doped graphene: (i) N/B atom on top of a Cu atom, (ii) B/N atom over a hollow site of the Cu substrate and (iii) all of the graphene atoms over hollow sites of the Cu substrate (Fig. S2). For N, the interaction with Cu is not dependent on the registry. All three regimes show a weak interaction between N p_z and Cu s and d states. For B, however, when the B or a C atom is on top of a Cu atom, and thus relatively close to the substrate, the B or C p_z orbital interacts directly with both dz^2 and s states on Cu, leading to a stronger interaction with the Cu substrate.

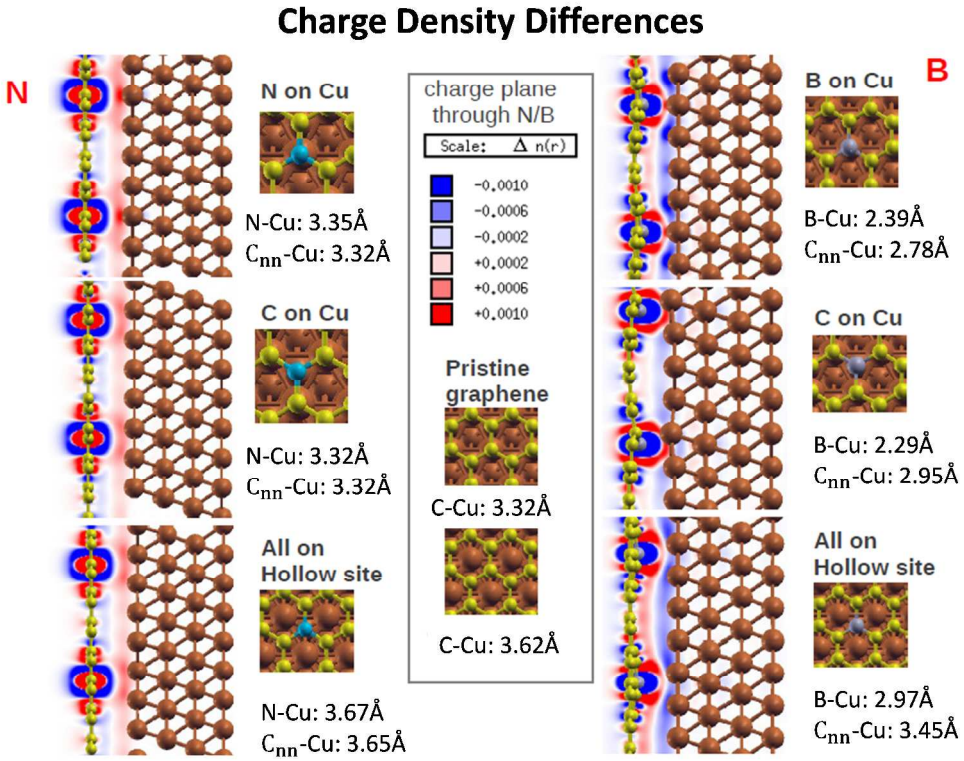

Fig. S2. Charge density differences between N (left panel) /B (right panel)-doped graphene and pristine (middle panel), with various registry between graphene film and Cu substrates.

We also investigate the effects of the substrate interactions on the local density of states. In Fig. S3, we show the projected density of states (pDOS) of p_z states for B (upper panel) and N (lower pannel) doped graphene with and without Cu substates. For the B-doped case, due to the interactions between B dopants and Cu substrates in type (i) and type (ii) registry, the DOS on the B dopant and the nearest neighbor C atoms are modified with respect to that of free standing B-doped graphene (without a Cu substrate). An extra peak is observed at about the Fermi level and 0.3eV below Fermi level in type (i) and type (ii) registry respectively. Meanwhile, the DOS of type (iii) registry is very close to that of free standing graphene, consistent with much less interaction in this registry. For the N-doped case, the DOS shows no dependence on registry between the graphene layer and Cu substrate, all of which is similar to that of the behavior of free standing N-doped graphene.

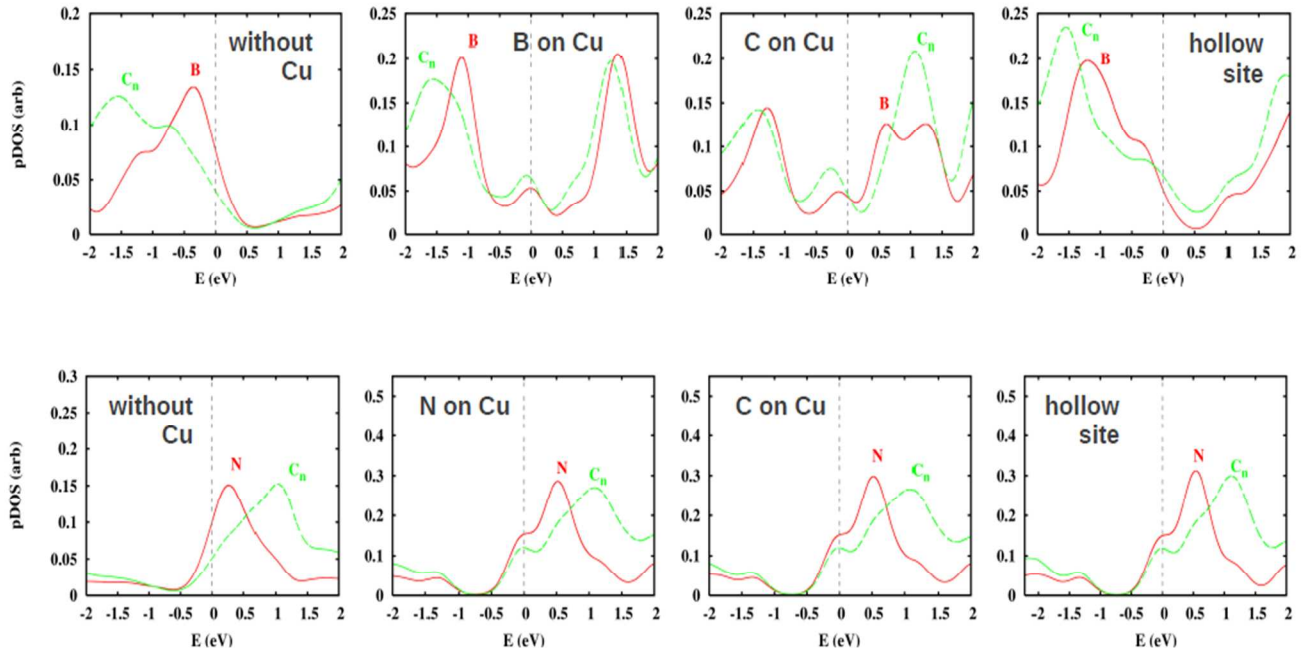

Fig. S3. pDOS of pz orbitals for B, N dopants and their neighboring C atoms in B (upper panel)/N (lower panel)-doped graphene, with various registry between graphene film and Cu substrates. pDOS for Cu surface states is also included in each situation.

Finally, we address the role of the distortion induced by the B interaction with the Cu substrate on the STM images. We simulated the STM image of a single graphitic B dopant in a graphene film, with the out of graphene plane distortion of the B dopant taken from the DFT structure on Cu(111) substrate, and the result is shown in Fig. S4 for a bias energy of -0.5 eV. The simulated result does not include the Cu atoms explicitly; rather, it incorporates the substrate's effect on the atomic structure. We find that this simulated result still matches the experimentally observed shape, a triangle pattern with the center at B dopant site and the three apexes at the first three neighboring C sites from B dopant. The spot with largest apparent height remains at B dopant site, but the height is slightly reduced, from ~0.92Å in free standing case to ~0.8Å in current case. Such a reduction of ~0.1Å is smaller than the physical distortion of 0.4Å, mainly due to the enhanced density of states at/around dopant sites after structural deformation. Fig. S4b and S4c show the projected density of states (pDOS) at B dopant, first, second and third carbon neighbors of B atom for the flat, free standing B-doped graphene and the distorted, free standing B-doped graphene on Cu substrate respectively. There will be further modification of the apparent height due to electronic interactions with the Cu substrate depending on registry, as illustrated in Fig. S3. In practice, the graphene is incommensurate to the substrate, but the general trend in Fig. S3 suggests a relative reduction in B pDOS in the -0.5 to 0.0 eV window.

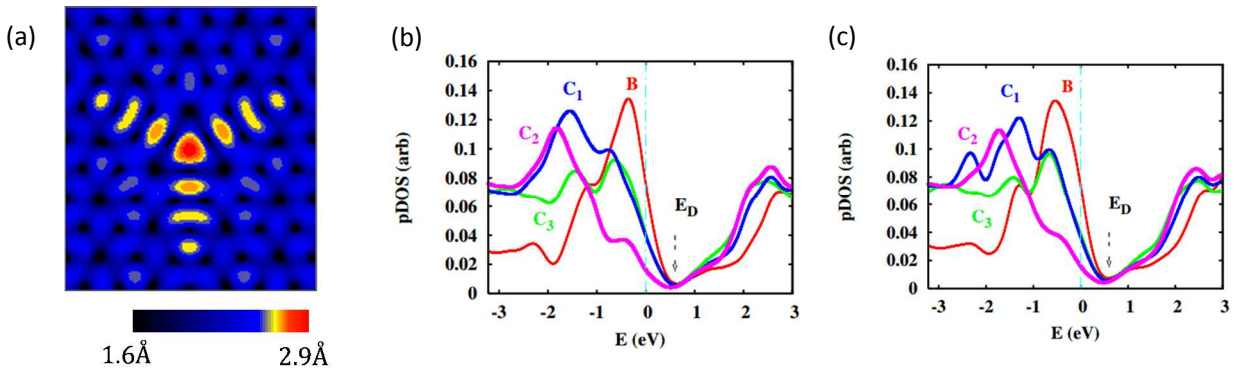

Fig. S4. (a) DFT simulated STM images for a single graphitic B dopant in graphene films on Cu(111) substrates at bias energy of -0.5V. (b) pDOS of B dopant, first, second and third carbon neighbors of B atom in free standing B-doped graphene. (c) pDOS of B dopant, first, second and third carbon neighbors in B-doped graphene on Cu substrate.

S3. Calculations of experimental value (p), expected value ($E(p)$) and standard deviation ($\sigma(p)$) for the ratio of dopants in one of the two sublattices.

The ratio of the number N_r of dopants in one sublattice out of a total of N dopants is defined as $p = \frac{N_r}{N}$. Under the hypothesis of a dopant occurring in both sublattices with equal probability, the ratio p follows a normal distribution with mean of $E(p) = 0.5$ and standard deviation of

$$\sigma(p) = \sqrt{E(p) \times (1 - E(p)/N}.$$

According to the definition above, we can get the experimental value of $p = 0.538$, expected value of $E(p) = 0.5$ and standard deviation of $\sigma(p) = 0.0462$ for Fig. 2d, and $p = 0.738$, $E(p) = 0.5$ and $\sigma(p) = 0.0453$ for Fig. 2e.

S4. Calculations of experimental value (I), expected value ($E(I)$) and standard deviation ($\sigma(I)$) for Moran's Index

In statistics, Moran's Index is used to measure spatial autocorrelation. It is defined as

$$I = \frac{N}{\sum_i \sum_j w_{ij}} \frac{\sum_i \sum_j w_{ij}(X_i - \bar{X})(X_j - \bar{X})}{\sum_i (X_i - \bar{X})^2}$$

In this formula, N is the number of spatial features which are indexed by i and j; $X_i (i = 1 \sim N)$ are the variables of interest for the i^{th} feature; $\bar{X}$ is the average of the variables; and w_{ij} is the spatial weight between the i^{th} and j^{th} features which is usually defined as the inverse of the distance between the two elements.

The expected value of Moran's Index under the null hypothesis of no spatial autocorrelation is

$$E(I) = \frac{-1}{N - 1}$$

And its variance is

$$\sigma(I) = \frac{NS_4 - S_3 S_5}{(N-1)(N-2)(N-3)(\sum_i \sum_j w_{ij})^2}$$

Where

$$S_1 = \frac{1}{2}\sum_i \sum_j \left(w_{ij} + w_{ji}\right)^2$$

$$S_2 = \sum_i \left(\sum_j w_{ij} + \sum_j w_{ji}\right)^2$$

$$S_3 = \frac{N^{-1}\sum_i (X_i - \bar{X})^4}{(N^{-1}\sum_i (X_i - \bar{X})^2)^2}$$

$$S_4 = (N^2 - 3N + 3)S_1 - NS_2 + 3(\sum_i \sum_j w_{ij})^2$$

$$S_5 = S_1 - 2NS_1 + 6(\sum_i \sum_j w_{ij})^2$$

In the example of Fig. 2d with 117 B dopants ($N = 117, i = 1{\sim}117$), 63 B dopants in one sublattice are assigned with a value of -1, while the remaining 54 B dopants in the other sublattice are assigned a value +1, as described below:

$$X_i = \begin{cases} -1 & when\ i\ is\ among\ the\ 63\ B\ dopants\ on\ sublattice\ A; \\ +1 & when\ i\ is\ among\ the\ 54\ B\ dopants\ on\ sublattice\ B. \end{cases}$$

Together with the calculated spatial weights between two features,

$w_{ij} = \frac{1}{r_{ij}}$ which is further normalized by $\sum_{i=1}^{N} w_{ij} = 1$

We can get the experimental value of $I = -0.019$, expected values of $E(I) = -0.0086$ and standard variation of $\sigma(I) = 0.0156$ for Fig. 2d, and $I = 0.066$, $E(I) = -0.0083$ and $\sigma(I) = 0.0159$ for Fig. 2e.

S5. Calculations for p-values of both tests of ratio and Moran's Index

As described in S1 and S2, both the ratio test and Moran's Index tests of given set of experimental data follow a normal distribution with a mean value of $E(p)$ [$E(I)$] and a standard deviation of $\sigma(p)$ [$\sigma(I)$], under the null hypothesis of dopants distributing randomly between two sublattices. Thus, $\frac{p-E(p)}{\sigma(p)}$ follows a standard normal distribution which is $\frac{p-E(p)}{\sigma(p)} \sim N(0,1)$ (here $N(0,1)$ stands for a standard normal distribution, $N(0,1) = \frac{1}{\sqrt{2\pi}} e^{-x^2/2}$). To measure the consistency between experimental observation and the null hypothesis, the p-value is introduced as $P(|Z| > \frac{p_0 - E(p)}{\sigma(p)})$, where p_0 is the experimental value, and $Z = \frac{p-E(p)}{\sigma(p)} \sim N(0,1)$.

For the B-doped case in Fig. 2d, the p-value obtained from the ratio test is 0.405, and from the Moran's Index test it is 0.503. For the N-doped case in Fig. 2e, the p-value for the ratio test is 1.5×10^{-7} and for the Moran's Index test it is 3.1×10^{-6}. We use the smaller value from the two tests to represent the likelihood of experimental results being consistent with the null hypothesis.

S6. Differential Conductance (dI/dV) taken far away from the SW defect sites

Shown in Fig. S4 is a "V" shaped dI/dV spectrum taken ~8 nm away from the SW defect sites. It clearly shows that Dirac point stays around Fermi level, indicating almost zero density of charge carriers in the graphene films.

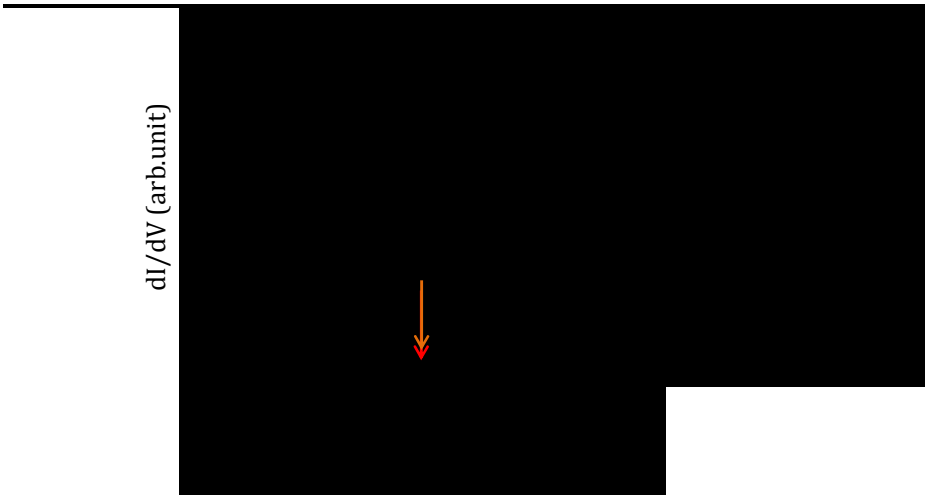

Fig. S4 dI/dV spectrum taken far away from the SW defect sites. Red arrow and Orange arrow point to the Dirac point and Fermi level respectively.

References:

1. Giannozzi, P.; Baroni, S.; Bonini, N.; Calandra, M.; Car, R.; Cavazzoni, C.; Ceresoli, D.; Chiarotti, G. L.; Cococcioni, M.; Dabo, I.; Corso, A. D.; Gironcoli, S. d.; Fabris, S.; Fratesi, G.; Gebauer, R.; Gerstmann, U.; Gougoussis, C.; Kokalj, A.; Lazzeri, M.; Martin-Samos, L.; Marzari, N.; Mauri, F.; Mazzarello, R.; Paolini, S.; Pasquarello, A.; Paulatto, L.; Sbraccia, C.; Scandolo, S.; Sclauzero, G.; Seitsonen, A. P.; Smogunov, A.; Umari, P.; Wentzcovitch, R. M. *Journal of Physics: Condensed Matter* **2009,** 21, (39), 395502.
2. Tersoff, J.; Hamann, D. R. *Physical Review B* **1985,** 31, (2), 805-813.
3. Vanderbilt, D. *Physical Review B* **1990,** 41, (11), 7892-7895.